ASSESSING FORE PARAMETERS FOR THE REBINNING OF 3D PET SCANS

M. Mazzoli*, E. De Bernardi*, F. Zito** and G. Baselli*

* Biomedical engineering Department, Polytechnic University of Milan , Milan, Italy
** Nuclear Medicine Department, Ospedale Maggiore Policlinico, Mangiagalli e Regina Elena, Milan, Italy

Corresponding author: elisabetta.debernardi@polimi.it

Abstract: A study for optimizing FORE parameters for the rebinning of 3D PET data into a stack of 2D sinograms is presented. FORE is based on a high frequency approximation (frequency-distance relation) which allows to assign acquired sinogram 2D Fourier Transform elements to the same elements of proper rebinned sinogram Fourier Transform. At low frequency, different rebinning methods must be used. To optimize the partitioning of the frequency space in FORE applicability and non applicability regions, we studied the validity of the frequency distance relation and obtained a validity map. The overlapping partition derived from the map was tested on acquired phantom data and showed to be able to reduce image artefacts due to the traditional disjointed partition.

Introduction

Fourier Rebinning (FORE), [1], is widely used in Positron Emission Tomography (PET) to reorganize data acquired without septa (3D mode) as if they were scanned with septa extended (2D mode). In 3D PET coincidences are accepted not only between nearly adjacent detector rings (direct sinograms, 2D mode), but also between distant detector rings (oblique sinograms), thus improving acquisition sensitivity. Rebinning algorithms allow the great amount of data generated by 3D acquisition to be reconstructed without increasing computation time. In fact, after rebinning, data can be reconstructed using fast algorithms usually applied to 2D data (Filtered Back Projection or iterative algorithms). At the moment, FORE is the most used rebinning algorithm because it offers a good compromise between accuracy and computation time requests.

FORE is based on the frequency-distance relation, [1,2], an high frequency approximation that allows the elements of oblique sinogram 2D Fourier Transform to be reassigned to the same elements of direct sinogram Fourier Transform at a proper axial distance. At low frequencies, different rebinning strategies must be used not to loose accuracy. Typically, the Single Slice Rebinning (SSRB) algorithm limited to a subset of low copolar acquisition angle data is used, as stated in [1].

In our experience we found that an abrupt subdivision between the high frequency FORE applicability region and the low frequency SSRB approximation region is the source of artefacts and loss in accuracy. A gradual partition of the frequency space in properly weighted overlapped regions could increase image quality.

Aim of this work was to assess the validity of the frequency-distance relation in the sinogram Fourier Transform space, in order to create a validity map. A further goal, was to assess the applicability of this map for a gradual transition on the rebinning strategy. The frequency space overlapped partition, obtained using a proper threshold on the validity map, was therefore tested on two experimentally acquired phantoms differing in frequency contents.

Materials and Methods

Review of frequency-distance relation and FORE derivation: In 3D PET a Line Of Response (LOR) connecting two detectors in coincidence is completely defined by four spatial coordinates: s, distance between the scanner axis and the projection of the LOR on the transaxial plane, φ, projection angle in the transaxial reference x,y (azimuthal angle), z axial coordinate of the LOR mid point, ψ, angle between the LOR and the transaxial plane (copolar angle). Coincidences corresponding to a fixed pair (z, ψ) constitute an oblique sinogram $p_{z,\psi}(s, \varphi)$; the oblique sinogram is called direct sinogram if ψ=0: Data corresponding to a fixed pair (φ,ψ) constitute a 2D projection $p_{\varphi,\psi}(s, z)$.

If f is the tracer spatial distribution inside the scanner Field Of View (FOV), the 2D Fourier Transform of an oblique sinogram can be expressed as, [1],

$$P_{z,\psi}(\omega,k) = \iint_{FOV} dxdy \int_0^{2\pi} d\varphi \cdot f(x, y, z + (-x\sin\varphi + y\cos\varphi)\tan\psi) \cdot \cdot \exp(-jk\varphi - j\omega(x\cos\varphi + y\sin\varphi)) \quad (1)$$

where ω is the radial continuous frequency corresponding to s and k the Fourier index corresponding to φ.

For large values of ω and k and for a fixed (x,y) coordinate couple, the phase of the exponential term in (1) varies quickly with φ and so the exponential term

ISSN: 1727-1983

oscillates rapidly between positive and negative values. The only exceptions are the neighbourhoods of the angles φ in which phase is stationary. Then, if the tracer distribution term varies slowly with φ, so along the axial direction, the inner integral in (1) can be approximated to zero outside the stationarity neighbourhoods, allowing its computation to be reasonably restricted only to those neighbourhoods. Phase stationarity angles have to verify equation (2):

$$\frac{k}{\omega} = x\sin\varphi - y\cos\varphi \tag{2}$$

Equation (2) admits two solutions if local consistency condition $|k/\omega| \le \sqrt{x^2+y^2}$ is satisfied; otherwise no stationary angles exist for the considered (ω,k,x,y) values, [2].
For large values of ω and k, the oblique sinogram 2D Fourier Transform can be consequently rewritten as:

$$\begin{aligned} P_{z,\psi}(\omega,k) &\approx \iint_{FOV} dxdy \int_0^{2\pi} d\varphi \\ &\cdot f\left(x,y,z-\frac{k}{\omega}\tan\psi\right)\cdot \\ &\cdot \exp(-jk\varphi - j\omega(x\cos\varphi + y\sin\varphi)) \\ &\approx P_{z-\frac{k}{\omega}\tan\psi,0}(\omega,k) \end{aligned} \tag{3}$$

The frequency-distance relation comes from equations (2) and (3) and states that the major contributions to an element (ω,k) of an oblique sinogram Fourier Transform come from activity sources located at a fixed distance $-k/\omega$ along the LORs from their mid point. This distance along the line of integration corresponds to an axial distance $-\tan\psi\ k/\omega$. This information is used by FORE algorithm to reorganize acquired data in a stack of direct sinograms: the (ω,k) element of the oblique sinogram (z,ψ) Fourier Transform is reassigned to the Fourier Transform of the direct sinogram of slice $z'=z-\tan\psi\ k/\omega$.

For the (ω,k) elements which satisfies the condition $|k/\omega| > R_{FOV}$, no stationarity angles exist for any (x,y) point inside the FOV. In this global non consistency region direct sinogram Fourier elements are nearly zero except the $(\omega\neq 0, k=0)$ elements which are definitely zero, [3].

In practical FORE implementation, the rebinned sinogram Fourier Transforms are estimated following equation (4).

$$\begin{aligned} &P_{reb}(\omega,k,z) = \\ &W_1(\omega,k)P_{FORE}(\omega,k,z) + W_3(\omega,k)P_{SSRB}(\omega,k,z) \end{aligned} \tag{4}$$

where masks $W_1(\omega,k)$ and $W_3(\omega,k)$ respectively define the high frequency region in which FORE can be used and the low frequency region in which SSRB has to be applied to data characterised by a small copolar angle. If applicability and non applicability regions are disjointed, $W_1(\omega,k)$ and $W_3(\omega,k)$ assume the form:

$$\begin{aligned} W_1(\omega,k) &= \begin{cases} 1 & ((k > k_{\lim}) \cup (\omega > \omega_{\lim})) \cap \left(\left|\frac{k}{\omega}\right| < R_{FOV}\right) \\ 0 & \text{otherwise} \end{cases} \\ W_3(\omega,k) &= \begin{cases} 1 & ((k \le k_{\lim}) \cap (0 < \omega \le \omega_{\lim})) \cup (\omega = k = 0) \\ 0 & \text{otherwise} \end{cases} \end{aligned} \tag{5}$$

where parameters $\omega_{\lim}$ and $k_{\lim}$ must be properly chosen. The obtained frequency space partition is shown in Figure 1 for the first quadrant.

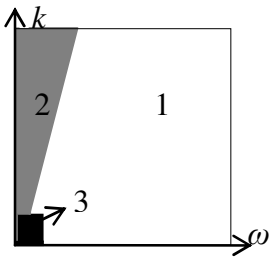

Figure 1: First quadrant direct sinogram frequency space partition: region1: FORE; region2: global non consistency; region3: SSRB to small copolar angle data.

Validity map analytical computation and frequency space consequent partition:. Our aim was to create a map of relative validity of the previously described approximations for each point (ω,k) of the 2D frequency space. This map had to be independent from the tracer spatial distribution and able to help the partitioning. To the point, an unique indicator, able to give a score to frequency-distance relation and to zero approximation validity in global consistency and non consistency regions respectively, had to be found.

After direct sinogram Fourier Transform estimate, the real part of the Inverse Transform is extracted and used for reconstruction. Then we studied the real part of the exponential term in (1):

$$\eta(x,y,\omega,k,\varphi) = \cos(\omega(x\cos\varphi + y\sin\varphi) + k\varphi) \tag{6}$$

In Figure 2, the function $\eta(x,y,\omega,k,\varphi)$ respect to azimuthal angle φ, together with the phase Φ of the exponential term in (1), is represented for two set of (x,y,ω,k,φ) coordinates. The first coordinate group satisfies the consistency condition, the second one doesn't.

ISSN: 1727-1983

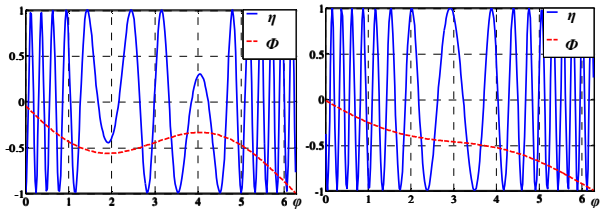

Figure 2: Example of $\eta(x,y,\omega,k,\varphi)$ and $\Phi(x,y,\omega,k,\varphi)$ respect to φ in consistency condition (on the left), and in non-consistency condition (on the right).

In consistency condition the frequency-distance approximation is the more valid the more the inner integral in (1) is equal to the integral computed in the stationarity angles neighbourhoods and so the more these neighbourhoods are narrow and the oscillations of $\eta(x,y,\omega,k,\varphi)$ outside them are fast. In non-consistency condition the goodness of the approximation requires the oscillations of $\eta(x,y,\omega,k,\varphi)$ to be as fast as possible.

The first momentum of the spectral density of $\eta(x,y,\omega,k,\varphi)$ in respect to φ was then chosen as unique indicator of goodness. For each frequency couple (ω,k) the validity $V(\omega,k)$ was computed as:

$$V(\omega,k) = \iint_{FOV} dxdy \frac{\int_0^{w_{max}} \left| \int_0^{2\pi} \eta(x,y,\omega,k,\varphi)\exp(-j\varphi w)d\varphi \right|^2 wdw}{\int_0^{w_{max}} wdw} \quad (7)$$

After normalising the obtained validity map in the range [0 1], the partition of the direct sinogram frequency space in overlapped regions was obtained defining $W_1(\omega,k)$ and $W_3(\omega,k)$ as:

$$W_1(\omega,k) = \begin{cases} 1 & (V(\omega,k)>T) \cap \left(\left|\frac{k}{\omega}\right| < R_{FOV}\right) \\ \frac{V(\omega,k)}{T} & (V(\omega,k) \le T) \cap \left(\left|\frac{k}{\omega}\right| < R_{FOV}\right) \\ 0 & \text{otherwise} \end{cases} \quad (8)$$

$$W_3(\omega,k) = \begin{cases} 1 - \frac{V(\omega,k)}{T} & (V(\omega,k) \le T) \cap \\ & \cap ((\omega > 0) \cup (\omega = k = 0)) \\ 0 & \text{otherwise} \end{cases}$$

where T is the threshold parameter to be suitably chosen.

Phantom studies: All the data were acquired with ECAT EXACT HR+ (CTI-Siemens) PET scanner. To make a first test of goodness of the obtained direct sinogram frequency space partition and to optimize the threshold parameter for the considered scanner, two phantoms filled with aqueous solution of ^{18}F were used. The first one was a line source of 2mm internal diameter and 9cm length. The line was placed in the central plane, radially oriented, and was scanned with its centre 22cm off axis. The second phantom was the Alderson thorax-abdomen phantom with districts filled with different activity, simulating the in vivo ^{18}F-FDG uptake. Spherical lesions of different radii (2.1, 4.1, 4.8, 5.1, 6.1, 11.0mm) were positioned inside.

All the data were rebinned with FORE and then reconstructed with 2D AWOSEM, (2iteration, 8 subsets), [4]. Reconstructed images were visually evaluated.

Results

The validity map $V(\omega,k)$ obtained evaluating the index defined in equation (7) is represented, for the first frequency space quadrant, in Figure 3.

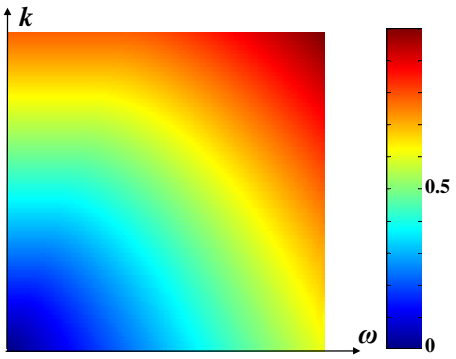

Figure 3: Validity map $V(\omega,k)$ obtained applying equation (7).

The map is consistent with the inapplicability of FORE at low frequencies.

The weighted overlapping masks $W_1(\omega,k)$ and $W_3(\omega,k)$, obtained applying equation (8) with T=0.125, are represented in Figure 4 for the frequency space first quadrant.

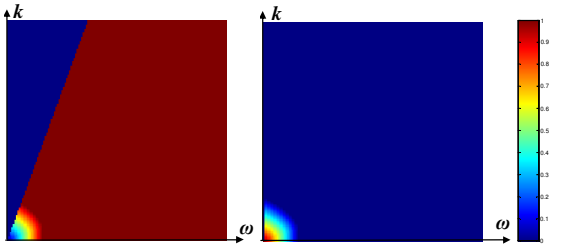

Figure 4: $W_1(\omega,k)$ and $W_3(\omega,k)$ for the frequency space first quadrant. Masks are obtained with T=0.125.

ISSN: 1727-1983

Results relevant to the two phantom studies are organized by comparing the following reconstructions: 1) the image obtained reconstructing only the low copolar data with SSRB; in this condition image quality is low, due to the noise component, but artefacts or distortions are completely absent. 2) reconstruction obtained after FORE rebinning with disjointed partitions of the frequency space and parameters $\omega_{lim} = 2\Delta\omega$ and k_{lim}.=2. 3) results obtained with the overlapped partition, with a value of threshold T=0.0625.

Transaxial reconstruction and axial section of the active line are respectively shown in Figure 5 and 6.

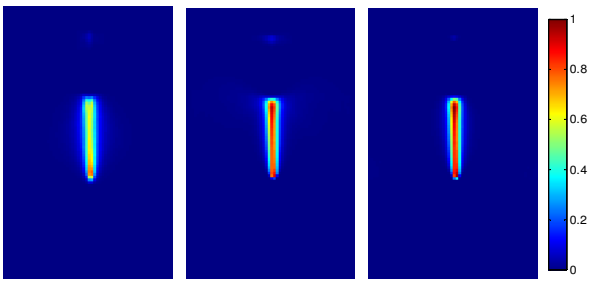

Figure 5: Transaxial reconstructions of the active line: SSRB applied to low copolar angle data+AWOSEM (left); FORE with disjointed partition (ω_{lim}=2$\Delta\omega$;k_{lim}=2) +AWOSEM (centre); FORE with overlapped partition (T=0.0625)+AWOSEM (right).

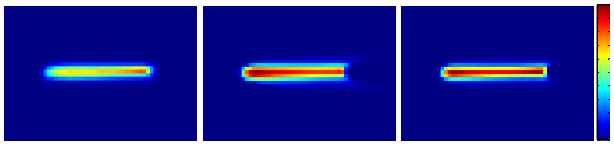

Figure 6: Axial section of the active line: SSRB applied to low copolar angle data+AWOSEM (left); FORE with disjointed partition (ω_{lim}=2$\Delta\omega$;k_{lim}=2) +AWOSEM (centre); FORE with overlapped partition (T=0.0625)+AWOSEM (right).

Alderson phantom reconstructions are reported in Figure 7.

Discussion

It's widely known that reconstruction of 3D data rebinned with FORE can lead to images characterised by the appearance of artefacts, [1,5]. Those artefacts are due to the hybrid nature of FORE. In fact the frequency-distance relation, on which FORE is based, is not valid over all the sinogram frequency space and then low frequencies must be differently rebinned. Usually, SSRB is used in this range, but, due to the large axial blurring it typically induces, its utilization is only limited to low copolar acquisition angle data. The artefacts are then due to the amplification of the low frequency elements which are characterised by a poorer signal to noise ratio. The extension of FORE applicability region towards low frequencies is able to decrease noise, but at the expense of an accuracy reduction. Generally, a compromise solution is obtained by choosing $\omega_{lim} = 2\Delta\omega$ and k_{lim}.=2, [1]. In our work we supposed that a further image quality degradation could have been due to the abrupt partition of the frequency space, which would have spread the low frequency noise component. The solution to overcame this problem could be a gradual frequency space partition into overlapped regions. Both abrupt and gradual partition could be done experimentally evaluating the effect of different arbitrarily chosen parameters on reconstructed images. In this work we tried to reduce this arbitrariness.

The first objective was the definition of an index able to quantitate FORE validity for each sinogram frequency space *(ω,k)* element. The real part of the inner integral inside oblique sinogram Fourier Transform expression was considered, and the spectral density respect to azimuthal angle was computed. Spectral density first momentum was chosen as validity index, because of its capability to assess the approximation level both in consistency and non consistency condition. The obtained map, by changing the unique threshold parameter, could help in optimizing the frequency space partition.

In the second part of our work we used the computed validity map to create a gradual partition of the frequency space in weighted overlapped regions. A visual inspection of the first results we reported seems to be in favour of our approach. In fact the presence of low frequency noise appears to be reduced on both phantoms. This demonstrates the applicability of the approach to various spatial activity distributions, thanks to the independency of the applied criterion from signal complexity.

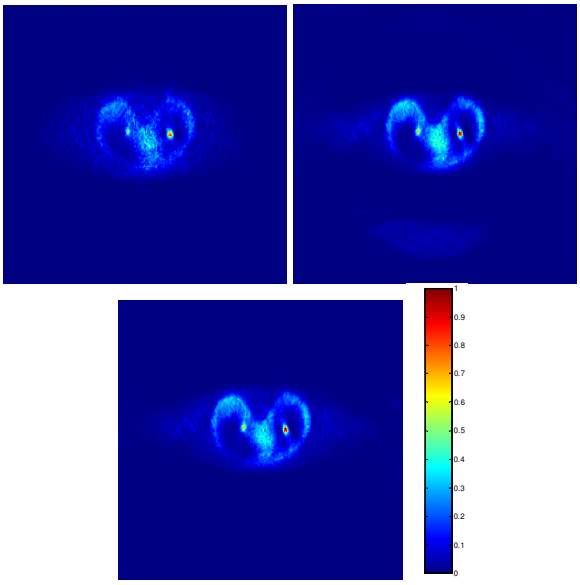

Figure 7: : Alderson phantom reconstructions: SSRB applied to low copolar angle data+AWOSEM (left); FORE with disjointed partition (ω_{lim}=2$\Delta\omega$;k_{lim}=2) +AWOSEM (centre); FORE with overlapped partition (T=0.0625)+AWOSEM (right).

ISSN: 1727-1983

Conclusions

Although a quantification of the approximation degree introduced by FORE in 2D reconstruction from 3D rebinned data involves a complex problem defined in the multidimensional space of sinogram frequencies and image axes, a valid, simple, and computationally efficient validity index was proposed and mapped on sinogram frequency space. Hence a criterion to define FORE applicability region in the domain where it operates was obtained. The introduction of a weight function for a gradual switch from the simpler SSRB (where FORE is not applicable) to FORE has given promising though preliminary results. Further validation over clinical data, mainly where oncological lesion have to be detected and evaluated, is needed, but significant improvement is foreseen in this application.

References

[1] DEFRISE M., KINAHAN P.E., TOWNSEND D.W., MICHEL C., SIBOMANA M. and NEWPORT D.F. (1997): 'Exact and approximate rebinning algorithms for 3D PET data', *IEEE. Trans. Med. Imag*., **16(2)**, pp. 145-158

[2] WEISHI X., LEWITT R.M. and EDHOLM P.R. (1995): 'Fourier correction for spatially variant collimator blurring in SPECT', *IEEE. Trans. Med. Imag*., **14(1)**, pp. 100-115

[3] DEFRISE M. and XUAN L. (1999): 'Fast and exact Fourier rebinning using John's equation', Nuc. Sci. Symp. Conf. Rec. 1999, **2**, pp: 869-873

[4] HUDSON H.M. and LARKIN R.S. (1994): 'Accelerated image reconstruction using ordered subsets of projection data', *IEEE. Trans. Med. Imag*., **13(4)**, pp. 601-609

[5] TANAKA E. and AMO Y. (1998): 'A Fourier rebinning algorithm incorporating spectral transfer efficiency for 3D PET', *Phys. Med. Biol*., **43(4)**, pp. 739-746

ISSN: 1727-1983